Determining the Architecture of the Terror Rift from Stratal Dips in Reflection Seismology Profiles

Research Thesis

Presented in partial fulfillment of the requirements for graduation *with research distinction* in Geological Sciences in the undergraduate colleges of The Ohio State University

By

Will Blocher

The Ohio State University
December 2013

Project Advisor: Professor Terry Wilson, School of Earth Sciences

Abstract

The Terror Rift is the youngest part of the West Antarctic rift system in the Antarctic interior. The Terror rift basin lies beneath the western Ross Sea near the Transantarctic Mountains. The rift has undergone multiple episodes of rifting, as evidenced by superimposed tilts of basin strata in fault blocks that define the rift. A younger tilt pattern has been superimposed on the rift around Ross Island, where the crust has flexed downward under the weight of young volcanoes. Mapping tilt directions provides a means to reconstruct the orientation of faults that produced tilt, and discriminate fault-induced tilt from younger flexure. This study is using seismic reflection profiles, imaging subsurface structure, to reconstruct tilts. Where two seismic lines cross, the true direction of tilt and the magnitude of tilt can be measured at multiple levels downward through the sequence of strata, such that changes in attitudes of bedding with depth can be determined. Maps of tilt directions from multiple crossing profiles for the time period marked by each seismic reflector will allow us to infer the orientations of these surfaces in 3D space. These orientations inform our knowledge of the dynamics of the episodes of rifting and volcano loading along the Terror Rift.

Geologic Setting and Background to the Research Problem

The Terror Rift manifests the most recent episode of rifting, or extensional deformation of the lithosphere, in the Victoria Land Basin of Antarctica. It is located between the Transantarctic Mountains and Ross Island (fig. 1). Much of the rift is expressed on the seafloor and, therefore, much of what we know of the rift comes from bathymetry of the sea floor and reflection seismology profiles acquired from ships.

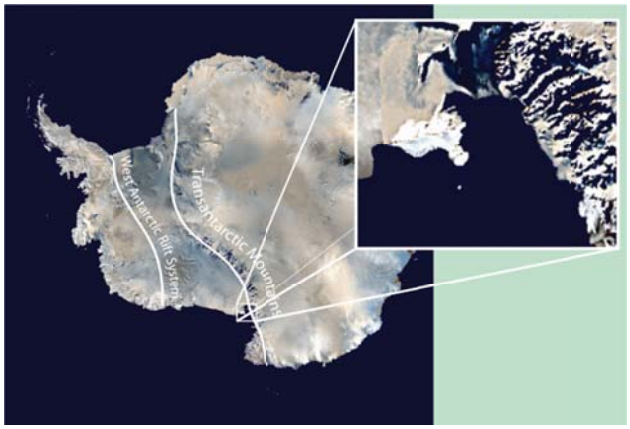

Fig. 1. The region of interest, the McMurdo embayment

An understanding of the geological evolution of the Terror Rift is critical to our understanding of the Antarctic Plate as a whole, as the genesis of this intra-plate deformation and the larger scale West-Antarctic Rift system is difficult to explain, and there is much contention in the academic community on the subject.

Previous studies of the region have mapped regional faults conventionally from reflection seismology profiles (by correlating interpreted faults from one profile to another)(Storti et al. 2008 and Salvini et al. 1997). From there, fault senses were ascribed and the region was determined to fit a larger-scale picture, tying the rift into the mid-ocean

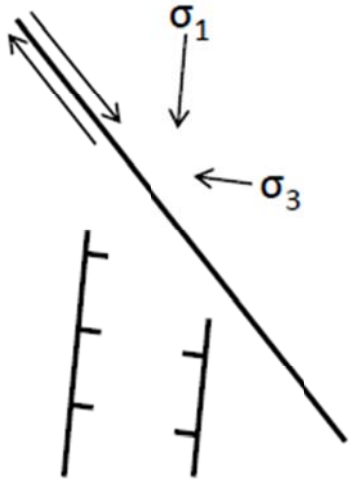

Fig. 2. A strike slip fault and associated riedel normal faults. From Storti et al. 2008

ridge as the normal component of a riedel shear system (fig. 2). Because this interpretation predicts such a geometrical relationship between these faults of different senses, and because descriptions of stress ellipsoids and of fault senses of motion are directly linked to their geometry accurately constraining the orientation of regional faults is critically important in the study of this rift system. However, several factors complicate the study of rift architecture in this area. First, images of the sedimentary layers in the subsurface acquired by reflection seismology are sparse in the area. Additionally, the sedimentary structures related to rifting were tilted from horizontal by the fault structures that broke the crust during rift deformation. A second phase of tilting was superimposed when the surface of the Earth flexed downward under the weight of the rift-associated volcanoes that make up Ross Island and the Erebus Volcanic Province. This study seeks to determine the nature of these structures and the stress conditions under which they formed.

The West Antarctic Rift system is the manifestation of the extension taking place in the Cenozoic, and the Terror Rift is its most recent expression (Salvini et al., 1997). The Cenezoic activity in the West Antarctic Rift system produced the Terror Rift, as first defined by Cooper et al. (1987). However, the dynamic and kinematic models for this rifting have not been extensively developed.

Study Approach, Data and Methodology

Approach

In studying any rift system, one of the main goals is to determine the orientation of stresses in the lithosphere at the time of deformation. The primary way of doing this is to look at the orientation of faults (brittle failure planes in the crust) associated with the episode of rifting. Fault geometry has a very strong and quantifiable relationship with stress orientation, and each can be predicted by the other.

The species of fault that characterizes a rift zone is the normal fault. Normal faults are brittle failures in the crust that accommodate horizontal extension. They feature shear displacement along slip surfaces that tend to dip at around 60°, the sense of which is hanging-wall down. Normal faults form in response to a strong, near-vertical stress (σ_1), and a relatively much weaker near-horizontal stress (σ_3), to which the strike of the fault is perpendicular (fig. 3).

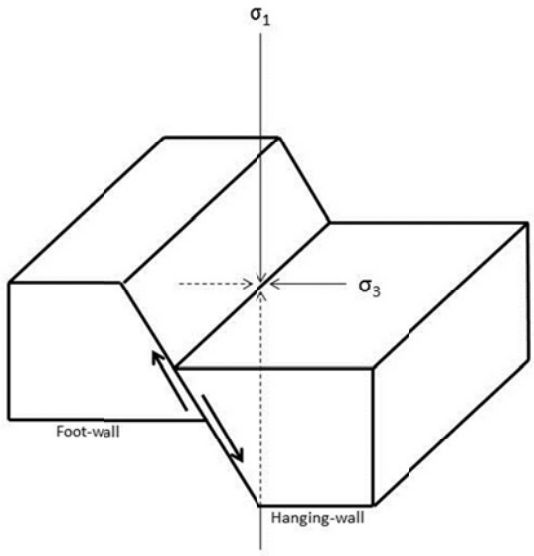

Fig. 3. The relationship between normal faults and the stresses that cause them.

Because of this relationship, a map of rift-associated normal faults in the region would be a very useful product, as it would strongly indicate stress directions within the crust during rifting. However, studying faults in and around McMurdo Sound is not straightforward as it is in many other places, because the rift system is submarine and subglacial, and the network of ship-born seismic lines is unfavorably diffuse.

Reflection seismic profiles are the main source of data for this study (fig. 4). A seismic profile is a 2-dimensional cross section of the Earth's crust. As an icebreaker tows its string of geophones, it emits a regular pulse of acoustic energy that is reflected and refracted in the subsurface to generate a profile of the basinal strata and structures (e.g. faults) that can be interpreted to inform us about the geometry of the Terror Rift.

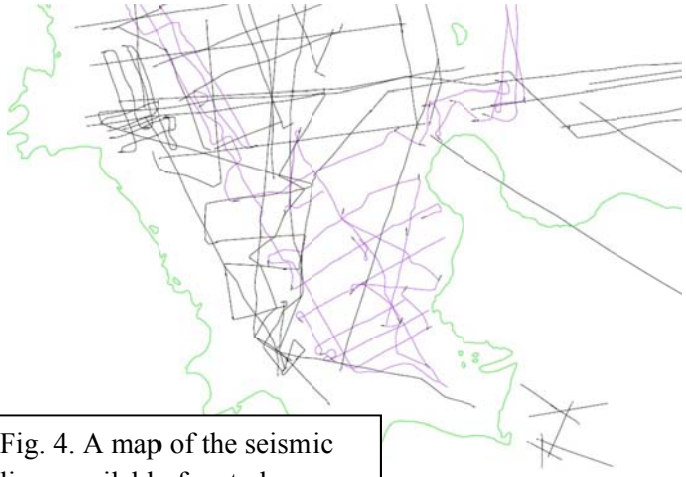

Fig. 4. A map of the seismic lines available for study.

A network of these 2-dimensional profiles can be interpreted and fleshed out into a three dimensional idea of the subsurface, but this requires the seismic lines to be sufficiently close together. If a fault is identified in one section, and that same fault is found in another section close by, the three-dimensional geometry of the fault can be approximated. However, the lines in the Ross Sea are sometimes spaced more than 30 kilometers apart, making such direct correlation of faults from line to line unreliable. Instead, my research seeks to make use of the seismic data through an understanding of the relationship of orientation relationship between sedimentary strata and the faults that cut them.

Both faults and flexure zones have characteristic signatures in stratal geometry. Both predict certain characteristics for strata deposited before, during, and after these episodes of deformation. All strata are initially deposited horizontally, but the faults that cut them typically curve at depth, imposing a rotation on the layers over the duration of slip along that fault. This means that the deepest strata (blue), those that the fault originally cut, are all parallel, but rotated a fixed amount. Above those strata are the strata that were deposited during the slip (orange), which are incrementally rotated, manifested as dip increasing with depth. These strata thicken towards the fault. Above are the strata deposited after any slip (not shown, which are parallel and un-rotated (horizontal))(fig. 5).

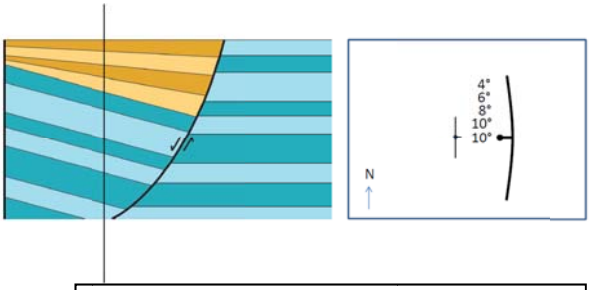

Fig. 5. A model depicting syn-rift strata (orange) and pre-rift strata (blue) associated with a listric normal fault. Dips recorded along the vertical line are displayed on the map.

Similarly, flexural loading produces rotation in underlying strata, which is expressed as a flexural moat approximating a circular downwarp around the point where the mass load is positioned. Within this moat are younger, unrotated strata (orange) that pinch out against the older (fig. 6). The signatures of faults and of flexure can be identified in vertical dip-profiles, and these vertical dip-profiles can be generated by means of the apparent dip problem.

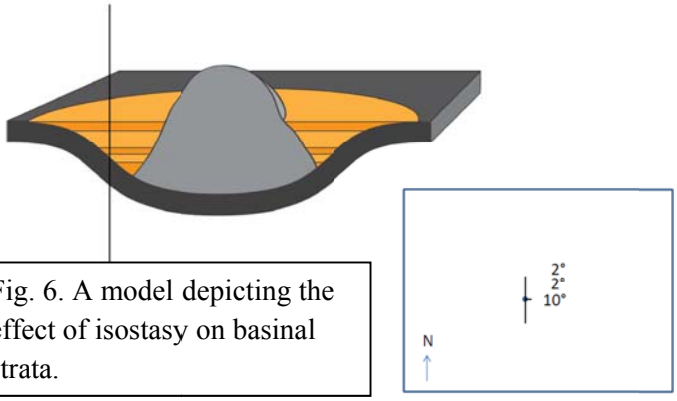

Fig. 6. A model depicting the effect of isostasy on basinal strata.

Seismic Reflection Profiles

The main building-block of a 2-D seismic profile is a vertical, 1-D "wiggle trace". A wiggle trace is a simple graph of amplitude over time recorded by a single geophone (or, more commonly, clusters of geophones) (fig. 7). A pulse of acoustic energy might take, for example, half of a second to travel from the signal source (in this case, an air-gun) to a particular, strong reflector in the sub-surface. What would be recorded is a pulse of reflected energy one second after the signal.

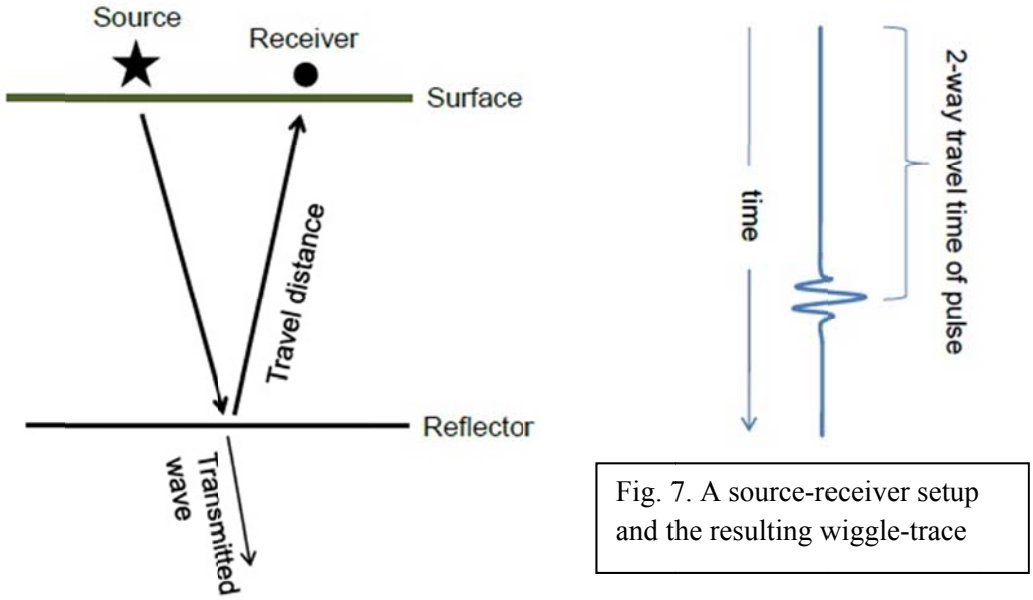

Fig. 7. A source-receiver setup and the resulting wiggle-trace

This is not, however, an in-depth "picture" of the subsurface, which is to say, a core taken at the same location might not show the same spatial distribution of strong reflectors. This is because all of the acoustic properties of the media through which the pulse travels must be accounted for.

Because sound does not travel through all media with the same velocity, there is no one factor by which you can scale a wiggle trace to make it a representation of reflectors with depth.

Fortunately, in my area of interest, some simplifications can be made. At large scales, the compression of deeper crust by lithostatic pressure increases the speed at which it transmits sound waves, because of the increase in its bulk modulus, i.e. its resistance to compression. However, because I am dealing with reasonably shallow depths, it can be assumed that the speed of sound does not change in a given medium with depth. Additionally, there are essentially only three acoustic velocities that I am obligated to pay attention to in this region – that of sea water, that of the basinal strata, and that of occasional volcanic intrusions. The basinal strata in this region all have very similar physical properties, due to their similar compositions and genesis. Because of this, it is reasonably safe to assume one constant velocity for all observed sedimentary units. Basinal strata are assumed to have an acoustic velocity of 2 meters / millisecond. The seawater above is assumed to have an acoustic velocity of 1.5 meters / millisecond.

One wiggle trace represents the journey of one packet of acoustic energy from source, to sub-surface, to receiver. An impulse of energy, generated at the ship, travels down through the water until it hits the seafloor, where it is split into a reflected and a refracted component. The reflected component travels back up and is collected at the surface by the geophone. That particular packet of energy has traveled twice the depth of the water (down and back up), the value of which can be determined by dividing by two and multiplying by the speed of sound in water. Meanwhile, the refracted component travels down through the upper-most rock units until it comes into contact with a strong reflector, where it is again split into a reflected and refracted component. The reflected component travels back up to the seafloor, is reflected/refracted, and is received by the geophone. This packet of energy has traveled down and back up through the water, but has also traveled down and back up through the thickness of

rock above the reflector. The distance from the ship to the reflector is therefore the distance to the seafloor, plus the amount of time between receiving the two signals, times the speed of sound in rock (fig. 8).

Methods

Formally, the expression for the depth of a reflector (D_R), in terms of the time-depth of the water (T_w) and the time-depth to the reflector (T_R) is as follows:

Eq. 1

$$D_R(m) = \frac{1.5\left(\frac{m}{ms}\right) \cdot T_w(ms) + 2\left(\frac{m}{s}\right) \cdot \left(T_R(ms) - T_w(ms)\right)}{2}$$

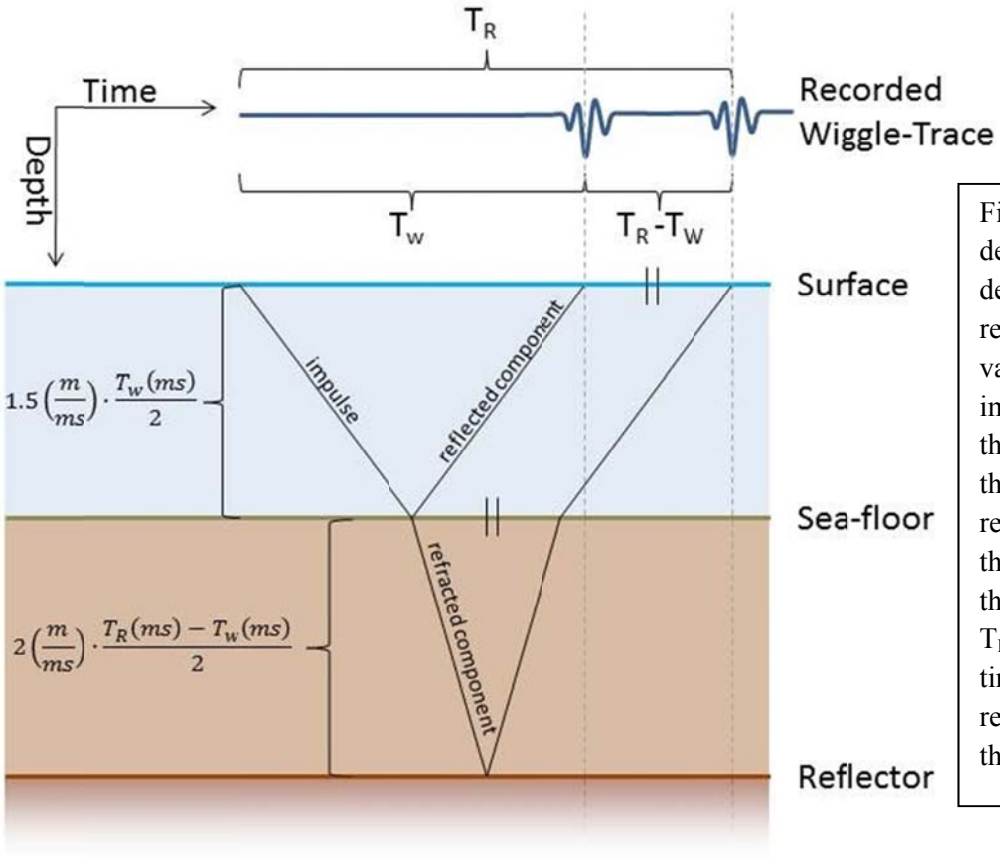

Fig. 8. In determining the depth to a reflector, the key variables are the impulse after T_w, the travel time of the wave that is reflected off of the seafloor, and the impulse after T_R, the travel time that is reflected off of the reflector.

This describes the conversion to depth of a single, 1-dimensional trace. A seismic section is nothing more than many of these vertical, 1-D graphs laid next to each other. Here is shown such a profile, with the strong reflectors examined in this study highlighted with various colors (fig. 9).

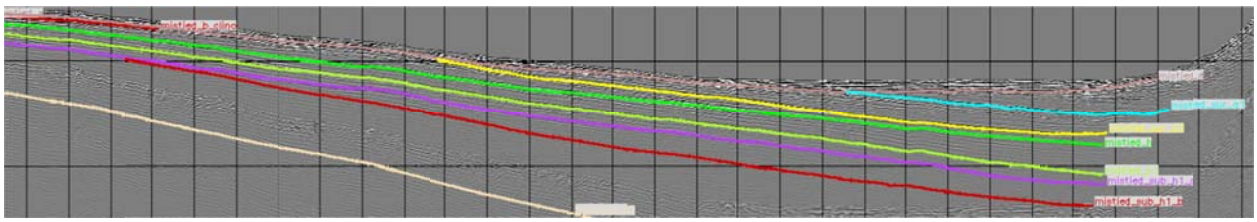

Fig. 9. An example seismic profile, depicting interpreted reflectors, displayed in GeoFrame 4.5

Key areas where the three-dimensional geometry of the sub-surface is known to a high degree of accuracy occur at the intersections of seismic lines. Instead of interpolating my 2-D profiles to come up with one 3-D picture, I've chosen to focus only on areas where the sub-surface geometry can be accurately determined – the intersections of seismic profiles – where I approximate the geometry of strata using three, 1-dimensional, vertical depth profiles – one at the intersection, and one on each seismic line, a short distance away from the intersection. The closer you are to an intersection, and the closer the two intersecting lines are to orthogonal, the more accurately you can determine the 3-D geometry of the sub-surface. However, it's only by chance that one of the sought-after faults might be located reasonably close to an intersection, so this property of the data is still not particularly useful in the direct mapping of faults. Instead, fault geometry can be determined indirectly from stratal geometry, which can be determined to a high degree of accuracy, at *any* seismic-line intersection.

The first step in the creation of a dip-profile is the creation of a fold-out. This is simply a

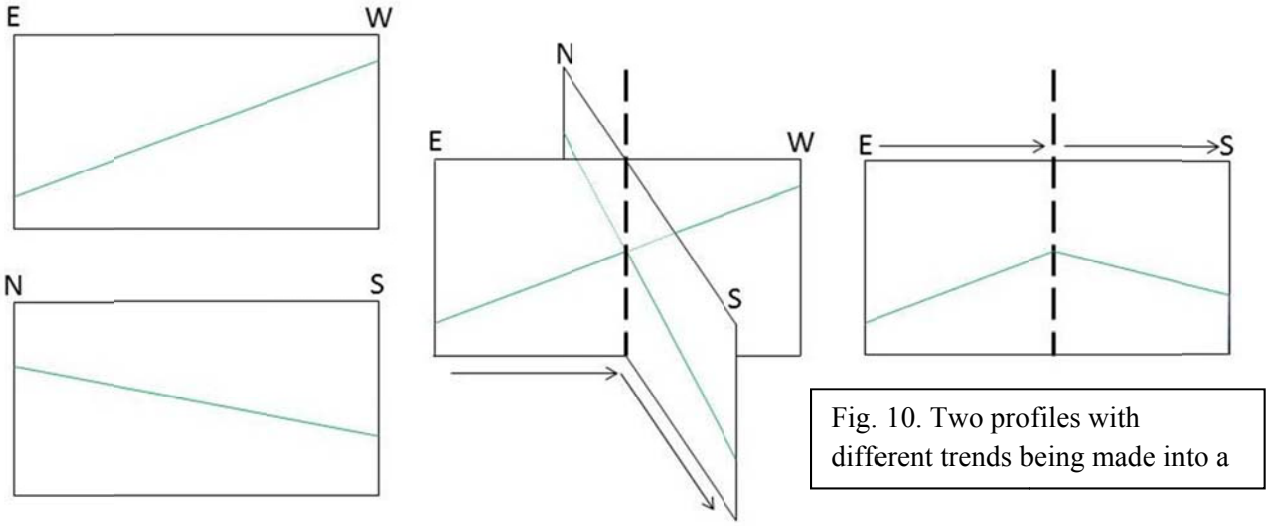

Fig. 10. Two profiles with different trends being made into a

visualization of the intersection of two seismic profiles. One profile is displayed on the left of the intersection of the profiles, or "fold-line", and the other is displayed on the right. Note that a fold-out is "flattened". In reality, the azimuths on either side of the fold-line are different (fig. 11).

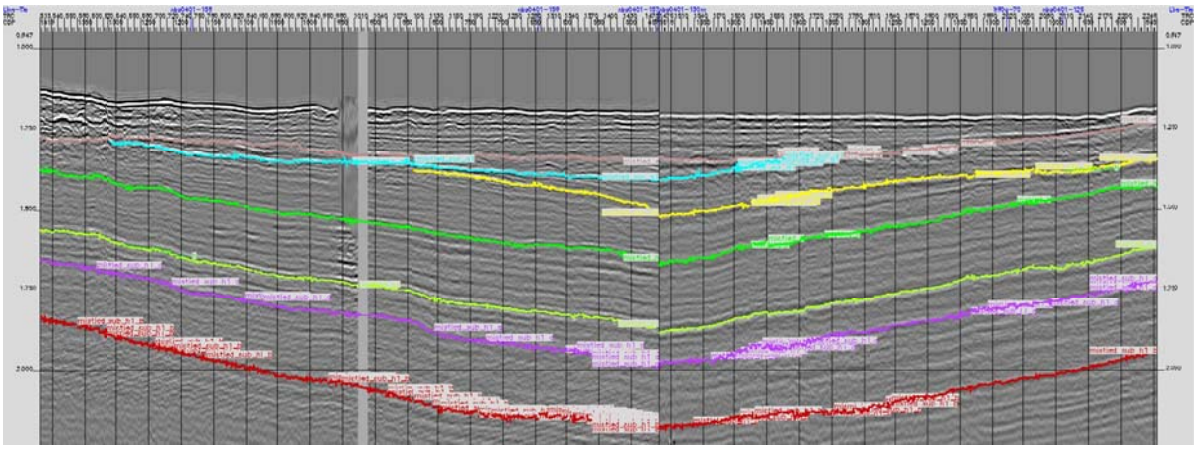

Fig. 11. A fold-out as it appears in GeoFrame 4.5

In profile, a reflector appears to dip one direction or the other, at a certain angle. However, this apparent dip does not represent the true dip of the bed, unless, by chance, the profile trends in exactly the dip direction of the bed. The true dip and dip direction of a given bed can be determined uniquely, if you know the apparent dip of the bed in at least two profiles trending in different directions. Thus, true dip of a given reflector can be determined mathematically at the intersections of seismic lines, and when this is done with a large number of reflectors at a common intersection, a with-depth profile of dips can be produced, and it is in these profiles that the signatures of faulting and flexure are detected.

First, three traces are chosen in the proximity of the fold-line, designated "A" on the left side of the fold-line, "B" on the right side of the fold-line, and the fold-line itself. The two-way travel times of each notable reflector, and of the seafloor, are recorded on each of the three lines. These travel times are then converted to true depths (D_A, D_{Fold}, and D_B) by eq. 1 (fig. 12).

Fig. 12. Time "depths" are recorded along A, Fold, and B and converted to true depths by eq. 1.

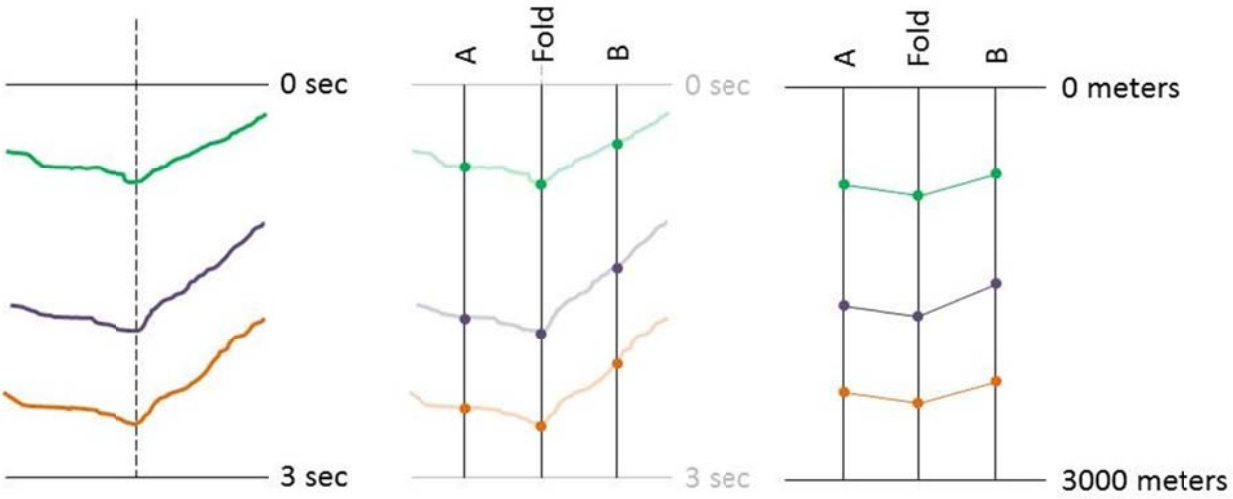

These lines are vertical, and therefore each has one unique latitude and longitude. From these three sets of coordinates, the horizontal distance from Fold to A (H_A) and that from Fold to B (H_B) can be calculated using the "haversine formula" (fig. 14).

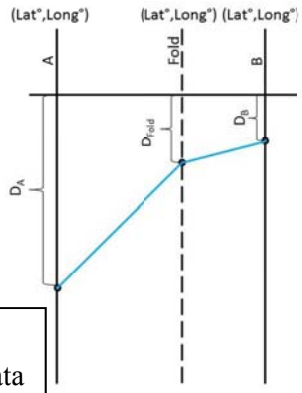

Fig. 13. Initial data

Eq. 2.

$$a = \sin^{2}\left(\frac{\Delta\varphi}{2}\right) + \cos(\varphi_1)\cdot\cos(\varphi_2)\cdot\sin^{2}\left(\frac{\Delta\lambda}{2}\right)$$

$$H = 2\cdot R\cdot \arctan 2\left(\sqrt{a}, \sqrt{1-a}\right)$$

Where φ is latitude, λ is longitude, and R is Earth's radius.

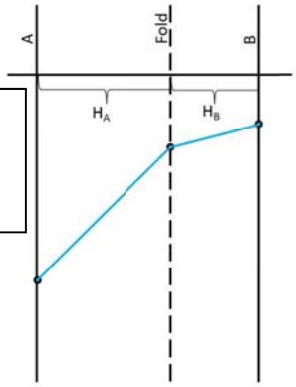

Fig. 14. Data derived from Eq. 2

This calculation is completed by loading the coordinates as points into ArcGIS.

Additionally, from the latitudes and longitudes is calculated the bearing from Fold to A (Θ_A) and the bearing from Fold to B (Θ_B) using the "initial bearing formula".

Eq. 3.

$$\theta = \arctan 2\left(\sin(\Delta\lambda)\cdot\cos(\varphi_2), \cos(\varphi_1)\cdot\sin(\varphi_2) - \sin(\varphi_1)\cdot\cos(\varphi_2)\cdot\cos(\Delta\lambda)\right)$$

This calculation is also done on tables within ArcGIS.

From H_A/H_B, D_A/D_B and D_{Fold}, the apparent dips of the reflector in the Θ_A and Θ_B directions can be solved by eq. 4. (Fig. 15)

Eq. 4.

$$\alpha = \arctan\left(\frac{D_{Fold} - D}{H}\right)$$

And finally, the strike and dip of the reflector at the fold-line can be calculated by solving the "two apparent dip" problem.

Eq. 5.

$$\theta_\delta = \arctan\left(\csc\left(\text{abs}(\theta_1 - \theta_2)\right)\left[\frac{\tan(\alpha_2)}{\tan(\alpha_1)} - \cos\left(\text{abs}(\theta_1 - \theta_2)\right)\right]\right) + \theta_1$$

$$\delta = \arctan\left(\frac{\tan(\alpha_1)}{\sin(\beta)}\right)$$

Where θ_δ is the true dip direction (90° from strike), θ_1 is the trend of the smaller apparent dip, α_1 is the smaller apparent dip, δ is the true dip, and β is the angle between strike and the smaller apparent dip.

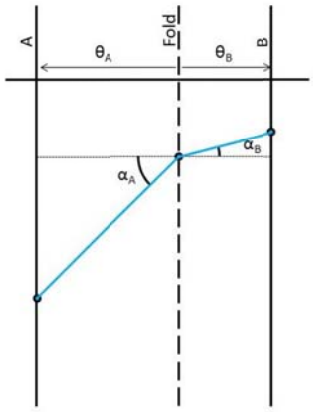

Fig. 15. Data derived from Eq. 3 and Eq. 4

Eight similar versions of these equations exist for cases when α_A is greater than or less than α_B, when α_A is positive or negative, and when α_B is positive or negative. (Fig. 16)

Fig. 16. Each of the eight cases has its own equation.

I've designated the classes (starting from the top-left): AV, BV, A\, B\, A/, B/, A^, and B^

A or B designates which angle is greater and V, \, /, ^ imitate the morphology of the foldouts determined by the angles' signs.

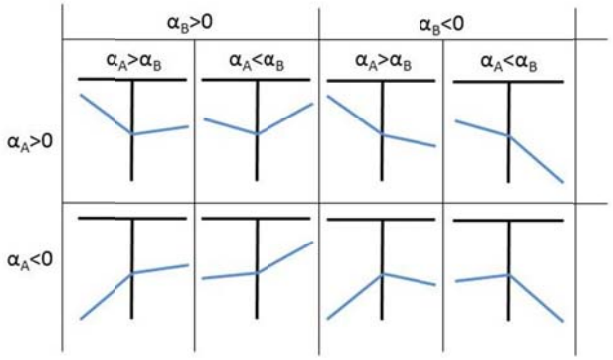

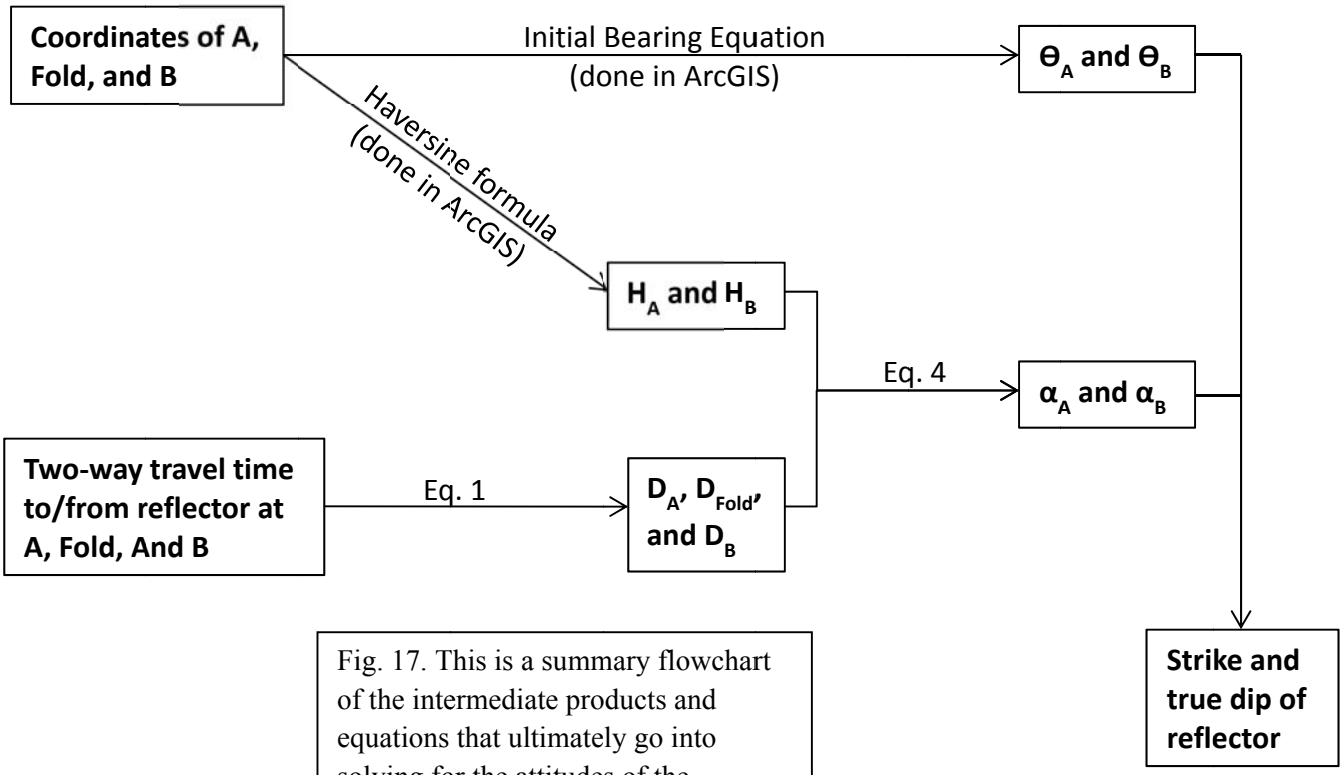

Fig. 17. This is a summary flowchart of the intermediate products and equations that ultimately go into solving for the attitudes of the reflectors.

Fig. 18. Block diagrams depicting the definitions of strike, dip, and dip direction, and the difference between dip and apparent dip.

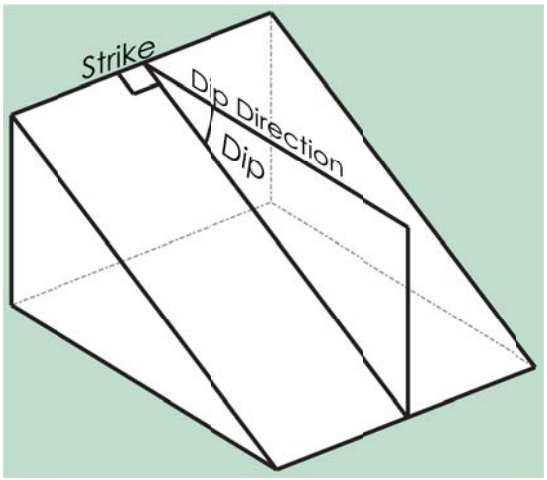

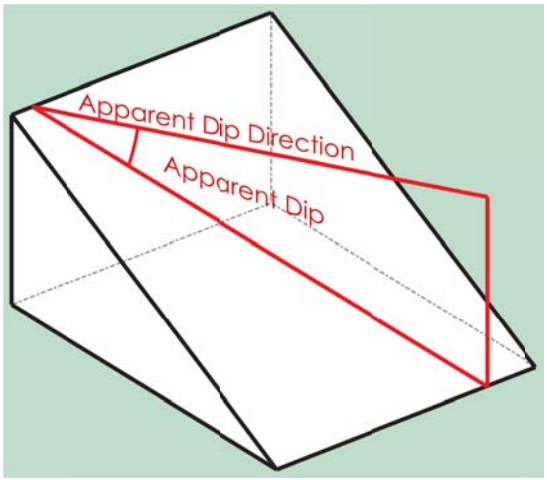

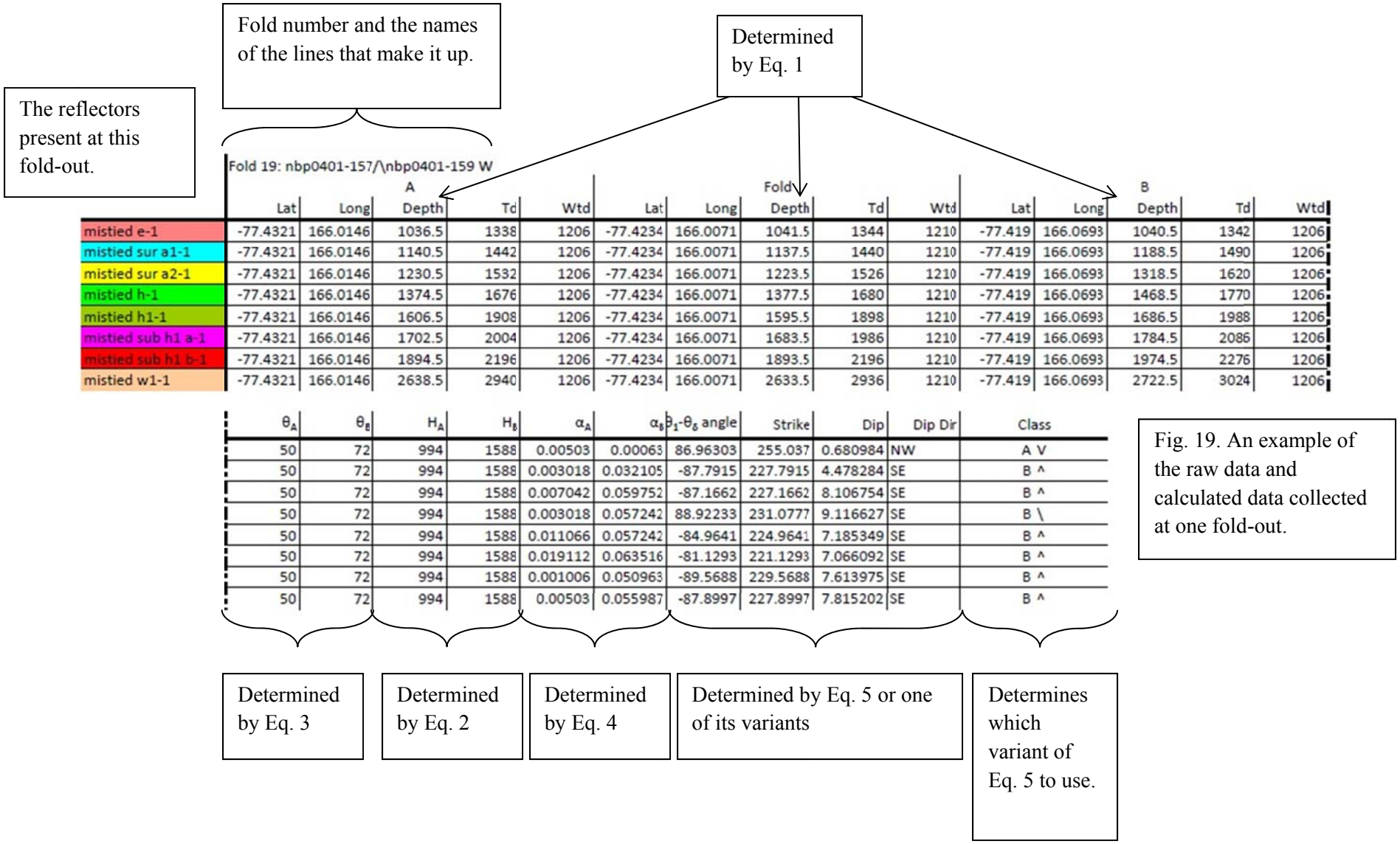

Fig. 19. An example of the raw data and calculated data collected at one fold-out.

Selecting Fold-Outs

There are several reasons a particular intersection might not be chosen for the creation of a fold-out. The first is that the vertical traces A and B may not be placeable. When solving for the attitude of the plane at the fold-line, it is important to pick and A and a B that are close to the fold-line, so that they are still representative of the local geometry. Further away, and the regional geology might see that a plane is not the best approximation, making the plane that is solved for less meaningful. However, A and B cannot be placed too close to the fold-line or the sensitivity of the calculations increases dramatically. All fold-outs from which data were collected had an appropriate place for A and B: close enough that they still represented the geometry at "Fold" and far enough away that +/- one pixel of vertical resolution along the wiggle trace corresponded to +/- one tenth of a degree in the calculations of alpha.

Additionally, a good fold-out candidate is made of two profiles in which key reflectors have been traced. If the reflectors are not traceable in one or more profiles, the calculations are impossible. There are two reasons that a reflector might not be traceable on a given profile. These are (1) that the sought after reflector occurs below the first "seafloor multiple" or (2) that the seismic data is skewed by the presence of volcanics.

The first reflection that a geophone receives is the reflection straight back from the sea floor. However, that impulse of energy is not done. The surface, being an air-water interface, is very conducive to the reflection of acoustic energy, as is the seafloor, a water-rock interface. Because of this, the source sound is reflected back and forth in the water column for the duration of the recording, showing up on the wiggle trace at regular intervals. At shallower depths, this interval is relatively short, yielding data that is highly obscured by the seafloor multiple.

Intersecting seismic lines must therefore be sufficiently far out from the shore to make for good fold-out candidates.

Volcanics also serve to obscure seismic data. Because sound travels faster through these rocks than the sedimentary basinal strata of interest, intrusions of igneous material skew the reflectors, making them appear sooner at the geophones than they would normally, yielding deceptively shallow depths. Igneous bodies' effects on the data can be calculated and subtracted in some areas, but in proximity to Ross Island, some of these features are so widespread and irregular that they can hopelessly obscure the data. (Fig. 20)

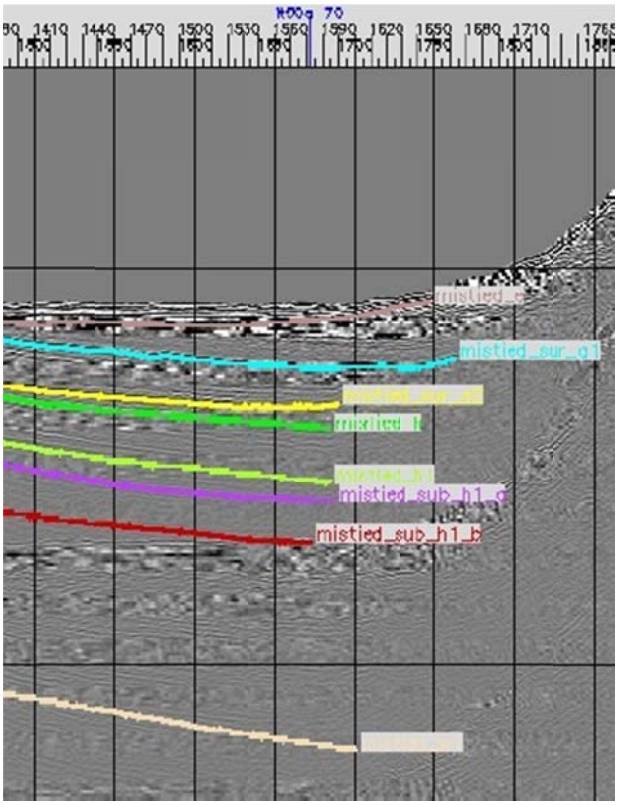

Fig. 20. An example of reflectors being lost in volcanics.

Results and Research Significance

Stratal 'true dip' directions have been calculated for a 8 reflectors at 20 seismic line intersections. These intersections have been plotted in ArcGIS at the longitude and latitude of their respective vertical fold lines (Fig. 21) and have been attributed tables containing the depths to, and dips / dip directions of all of the reflectors that intersect that line. An abbreviated map displaying these data as coincident dip symbols appears below. The reflectors " h-1" (green, the shallowest of the three), "sub h1 a-1" (purple), and "w1-1"(beige, the deepest of the three) were

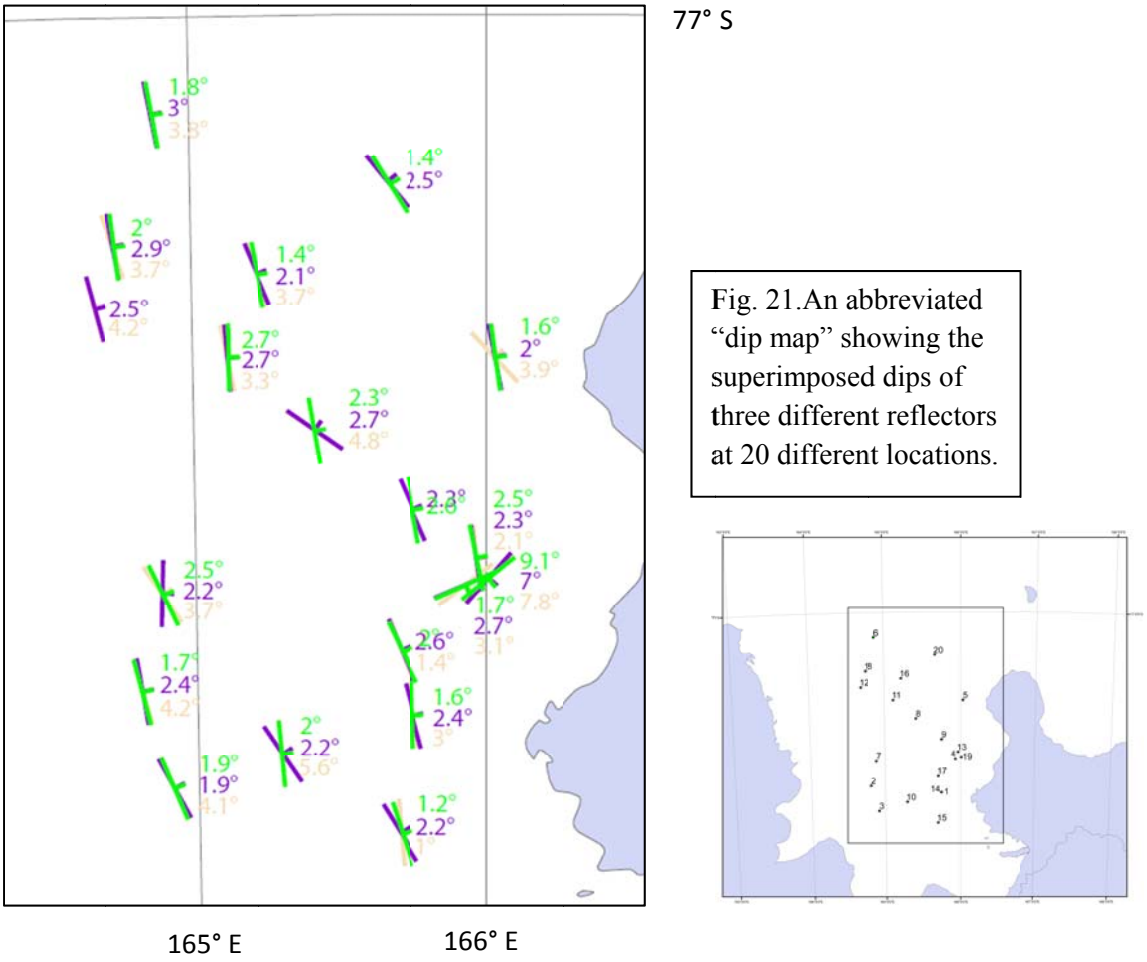

Fig. 21.An abbreviated "dip map" showing the superimposed dips of three different reflectors at 20 different locations.

selected for this map because of their representation of a wide range of depths and because of their lateral extensiveness (the appear on nearly every fold-out).

These results yield patterns that strongly express signatures of tilting by faulting and by flexure. Both structures share an increasing dip with depth, and this is expressed at every fold-out. Far out in the embayment, the dips increase gradually with depth, displaying the fanned morphology of syn-tectonic faulted strata. This histogram (Fig. 22) depicts the trend, with the peaks of the distributions of dips shifting towards lower numbers in more and more recent reflectors.

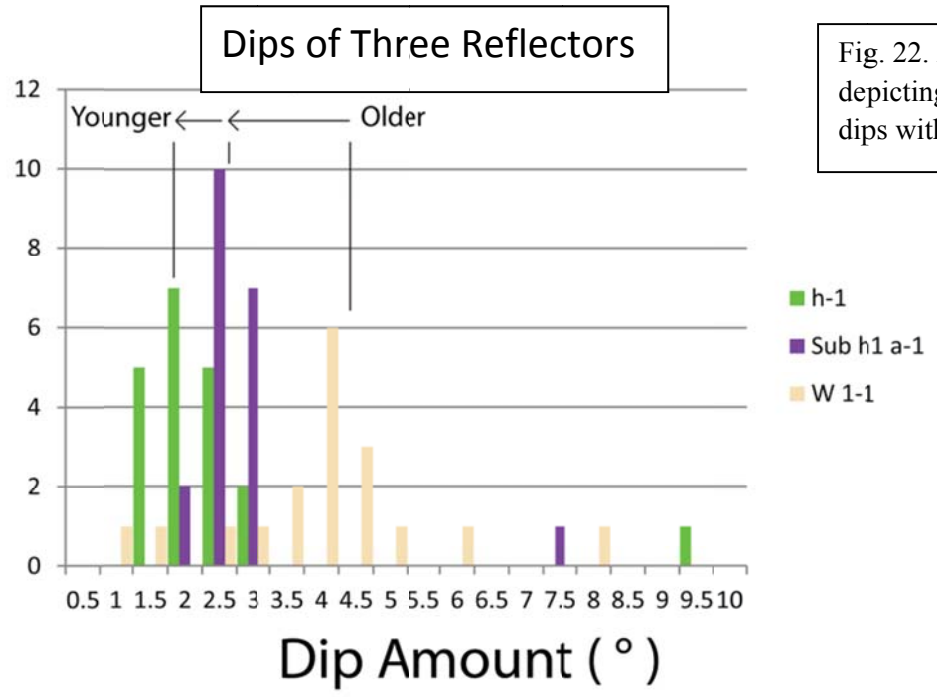

Fig. 22. A histogram depicting the change in dips with depth.

Additionally, the near-uniform dip directions suggest a particular fault orientation, and therefore a particular stress state. However, approaching Ross Island, the dip profiles begin to change subtly. First, and most obviously, the dip directions begin to shift toward the volcanos that make up the island. Secondly, the contrast between the dips in older and younger reflectors is larger and more sudden. And thirdly, the youngest reflectors observed are confined to this region ("e-1" and "sur a1-1", the youngest reflectors, only appear on foldouts 4, 5, 13, and 19 (refer to fig. 16. For these locations)).

This is interpreted to reflect a transition from rift-controlled geometry in the West, to flexure-controlled geometry in the East. The uniform strike, fanned strata represent the rift-controlled region, while the western fold-outs can more easily be explained by isostasy from the volcanos of Ross Island. The sharpness of the changes in dip in the western fold-outs is a reflection of the relatively short timescale over which the loading is imparted. The creation of the relevant volcanos took place over a short enough timespan that there isn't a significant package of strata that can be described as syn-isostatic. Instead, there are the relatively steeply dipping, pre-isostatic strata, and the relatively flat-lying post-isostatic strata that truncate into them. However, the lower, pre-isostatic strata, are also fanned, with gradually changing dips among themselves. This suggests that this isostatic structure, called a "flexural moat" was actually super-imposed onto syn-rift strata.

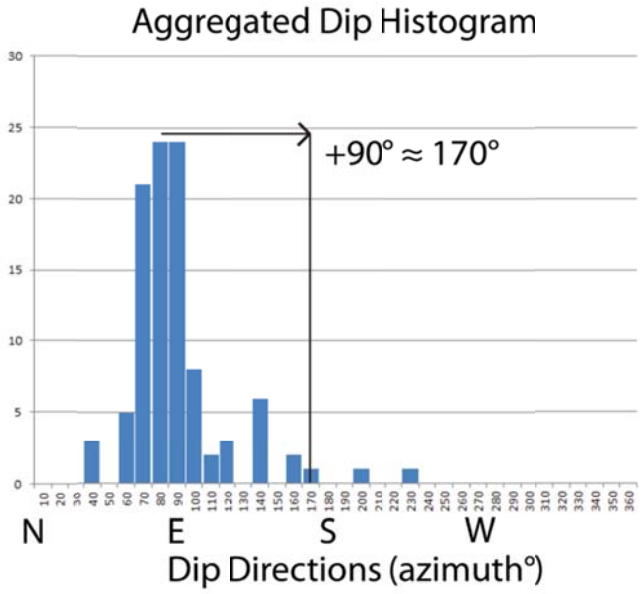

Fig. 23. A histogram predicting the strike of the normal faults that rotated the strata..

By examining the attitudes of the strata in the eastern, rift-dominated region, the orientation of faults can be indirectly determined. Because fault blocks tend to rotate about an axis that is parallel to the associated fault, the dip directions of rotated strata tend to trend perpendicular to the strike of the faults that rotated them. I have created a histogram of dip directions of all reflectors, except for those super-imposed with the flexural moat (Fig. 23). Shifting its peak 90° gives an estimate of the strike of the normal faults associated with the rift. In the case of the Terror Rift, this estimate is 170°.

In addition to the implied, rift-dominated region, there is a superimposition of the flexure imparted by the volcanos of Ross Island, which is visible in the data. The dips are steeper and the strikes vary slightly, suggesting that the strata have been rotated twice. Also, the lateral extent of two of the youngest reflectors shows a radial relationship with Mt. Bird (fig. 24).

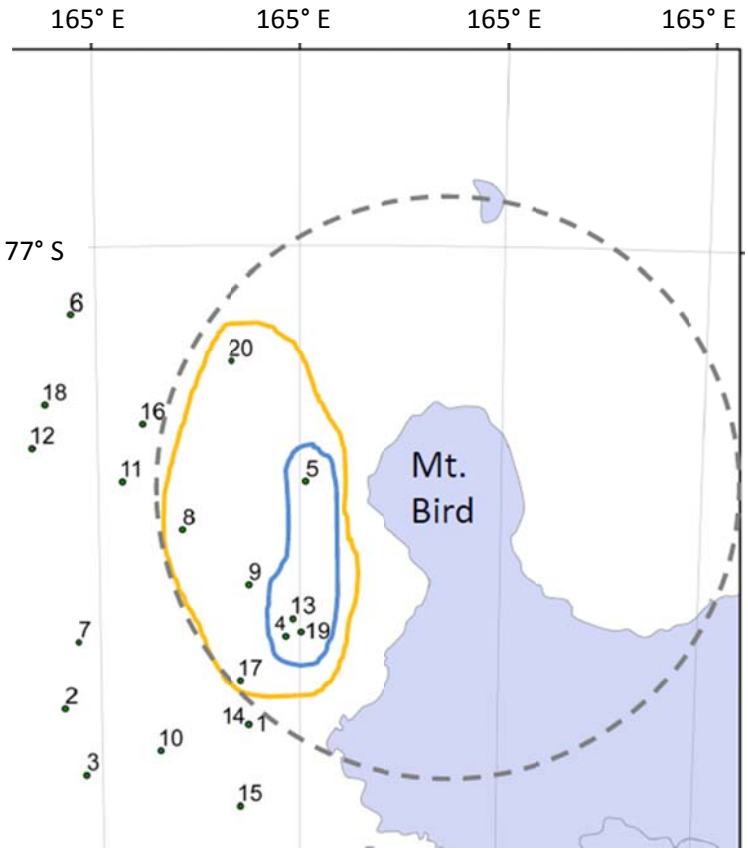

Fig. 24. A map depicting the appearances of "sur a1-1" (blue) and "sur a2-1" (yellow)

Even without a map of faults, the attitude of the faults that make up the Terror Rift can be constrained to some degree. The horizontal extension suggests a dip of 60° east / west, and the characteristics of syn-rift strata suggest a regional strike of about 170°. From this information and knowledge of the relationship between stresses and the faults they form, it can be determined that the greatest principal stress at the time of the formation of the rift was near vertical and the least principal stress was 80° / 260°. The results from this study have quantified the directions of the forces associated with rifting and flexure of the Earth's crust in this dynamic intraplate region.

Possibilities for Future Research

The reflectors observed in this study are able to be traced to two boreholes from which core has been taken (Wilson et al., 2012). Incorporating this information into this study's morphological description of the region could inform us about the timing of the imposition of rift and flexure structures.

Additionally, while the area in the immediate proximity of Ross Island is the most difficult to generate fold-outs in, it remains the most interesting, due to the double-rotation of strata by rifting and loading. More data, obtained possibly by revised methods, should be acquired in this region.

Acknowledgements

I would like to thank my family for supporting me throughout my undergraduate career, Dr. Terry Wilson for her guidance and seemingly infinite knowledge and wisdom, and the entirety of her research team for their support.

I would also like to thank the National Science Foundation for the funding of the collection of the reflection data used in this study, and Schlumberger for the academic license of Geoframe 4.5 used to interpret it.

References

Aitken, Alan R.A., G.S. Wilson, T. Jordan, K. Tinto, H. Blakemore (2012) Reprint Of: Flexural Controls on Late Neogene Basin Evolution in Southern McMurdo Sound, Antarctica. *Global and Planetary Change* 96 - 97: 9-22

Cooper, A. K., F. J. Davey, and J. C. Behrendt, (1987), Seismic stratigraphy and structure of the Victoria Land basin, western Ross Sea, Antarctica. In: Cooper A.K. and Davey F.J. eds., The Antarctic Continental Margin: Geology and Geophysics of the western Ross Sea. Published by theCircum-Pacific Council for Energy and Mineral Resources, Houston, Texas, 5B, 27-66

Salvini, F., G. Brancolini, M. Busetti, F. Storti, F. Mazzarini, and F. Coren (1997), Cenozoic Geodynamics of the Ross Sea Region, Antarctica: Crustal extension, intraplate strike-slip faulting and tectonic inheritance, J. Geophys. Res. 102: 669 – 696

Storti, F., M. L. Balestrieri, F. Balsamo, and F. Rossetti (2008), Structural and thermochronological constraints to the evolution of the West Antarctic Rift System in central Victoria land, *Tectonics* 27, issue 4: 82-93

Wilson, Gary S., R.H. Levy, T.R. Naish, R.D. Powell, F. Florindo, C. Ohneiser, L. Sagnotti, D.M. Winter, R. Cody, S. Henrys, J. Ross, L. Krissek, F. Niessen (2012), Neogene Tectonic and Climatic Evolution of the Western Ross Sea, Antarctica — Chronology of Events from the AND-1B Drill Hole." *Global and Planetary Change* 96 - 97: 189-203

Fold-line Locations

ID	Lat	Long
1	-77.5256	165.746
2	-77.5053	164.8116
3	-77.5785	164.9171
4	-77.4285	165.9304
5	-77.2578	166.0304
6	-77.073	164.8765
7	-77.4328	164.887
8	-77.3112	165.4135
9	-77.3719	165.7486
10	-77.5534	165.2928
11	-77.2568	165.1182
12	-77.2188	164.6773
13	-77.4088	165.9682
14	-77.5257	165.7445
15	-77.6142	165.7008
16	-77.1944	165.2237
17	-77.477	165.7054
18	-77.1716	164.7414
19	-77.4234	166.0071
20	-77.1257	165.6651

e-1			
Fold	Strike	Dip	DD
1	180.5288342	1.49110296	E
4	42.78110334	0.540163048	SE
5	285.6786544	0.266458982	SW
6	164.380171	0.509865624	NE
7	175.5284418	1.351838665	E
8	128.2750929	1.678253104	NE
9	162.2319149	1.104660957	E
10	183.2095364	3.267234601	E
11	183.0293105	1.724572165	E
12	23.92922083	1.037861348	E
13	316.0584907	1.021024084	NE
14	171.0118895	1.621736704	E
15	356.5249332	0.412098829	W
16	191.464212	0.910651399	E
17	150.8727817	0.672488038	E
18	161.1566611	0.149677448	E
19	255.0369708	0.680984278	NW
20	185.8346406	0.31540336	E

sur a1-1			
Fold	Strike	Dip	DD
4	49.82192461	1.047752287	SE
5	173.2393516	1.615360703	NE
13	177.7109304	1.887658704	E
19	227.7915355	4.478283743	SE

sur a2-1			
Fold	Strike	Dip	DD
4	61.45404807	1.66530036	SE
5	177.4618079	1.253277069	NE
6	168.1821378	1.666730942	NE
8	143.6005868	3.319298198	NE
9	138.944904	3.501469277	E
13	152.9869718	3.296647321	E
19	227.1661601	8.106753925	SE
20	202.3079833	1.504255488	E

h-1			
Fold	Strike	Dip	DD
1	178.6449123	1.642478194	E
2	167.0675816	1.685778777	E
3	158.9404455	1.882225073	E
4	65.81121996	1.738219885	SE
5	172.3977415	1.593018635	NE
6	171.5491707	1.840483699	NE
7	153.9884575	2.467278282	E
8	170.3448164	2.315083073	E
9	170.4603061	2.645225257	E
10	175.3442141	2.038720885	E
11	181.2856625	2.668708535	E
12	23.92922083	1.037861348	E
13	168.2706264	2.483998623	E
14	190.5539939	1.476248459	E
15	162.1216944	1.207365651	E
16	169.1087212	1.366010739	E
17	153.7568622	2.058845922	E
18	174.6044795	1.975013914	E
19	231.0776671	9.116627331	SE
20	148.3922418	1.352735976	E

h1-1			
Fold	Strike	Dip	DD
1	167.2103411	1.896056313	E
2	177.8570303	2.437324597	E
3	152.3380092	1.624846764	E
4	57.72627467	2.608741419	SE
5	171.0040269	2.268200156	NE
6	176.2045584	2.672385755	NE
7	184.3990982	2.626956731	E
8	158.3296408	2.448841559	E
9	162.5804495	2.705816738	E
10	162.506417	2.206816099	E
11	175.0902337	2.6198378	E
13	164.9058163	2.352265267	E
14	161.9340233	1.830401848	NE
15	171.9684137	2.585228826	E
16	163.8268207	1.85410065	E
17	157.1639276	2.230850768	E
18	168.9927923	2.446657182	E
19	224.9640907	7.185348615	SE
20	132.5241144	2.919059281	E

sub h1 a-1			
Fold	Strike	Dip	DD
1	165.2861619	2.416633653	E
2	171.8666177	2.40797213	E
3	152.3369139	1.881018659	E
4	66.76943198	2.656081913	SE
5	168.6902816	2.009694981	NE
6	170.5634122	2.997692058	NE
7	183.1702241	2.233091904	E
8	125.9369142	2.652211082	NE
9	154.5551931	2.288775409	E
10	146.9141034	2.184643929	E
11	176.843155	2.716047697	E
12	166.6088973	2.540843364	E
13	171.0415806	2.348077566	E
14	158.0547063	1.911137832	NE
15	148.3488625	2.219768409	E
16	158.2269313	2.14635872	E
17	156.5481814	2.555350701	E
18	171.2630374	2.887820803	E
19	221.1292576	7.066092142	SE
20	141.1030496	2.456195502	E

sub h1 b-1			
Fold	Strike	Dip	DD
1	167.2485575	2.355410421	E
4	68.31908068	2.258754606	SE
5	167.6491702	1.761698154	NE
6	181.1322464	3.711148765	NE
7	180.6915381	1.901857382	E
8	159.1694631	3.370292517	E
9	154.9929662	3.413374626	E
10	189.0574747	4.009577492	E
11	170.7004841	3.335680974	E
12	163.6337063	2.939661734	E
13	158.3364344	2.736358677	E
14	154.8523919	2.075126804	NE
15	161.1852039	2.309459474	E
16	160.169562	2.575534299	E
17	157.840922	3.378938778	E
18	165.4700726	3.339018289	E
19	229.5687943	7.613975486	SE
20	148.569021	2.322088179	E

w1-1			
Fold	Strike	Dip	DD
1	173.7582102	2.985201496	E
2	165.333144	4.178022069	E
3	156.3582874	4.082206025	E
4	52.21173241	3.083376574	SE
5	136.9568716	3.892482916	NE
6	170.8645601	3.779962311	NE
7	157.6065462	3.709544724	E
8	125.4572535	4.761296425	NE
10	175.4482674	5.552284207	E
11	169.8822849	3.323595766	E
12	167.3120015	4.210993403	E
13	174.8854111	2.08293354	E
14	156.6289283	3.596835337	NE
15	174.9883566	0.884261042	E
16	163.8567403	3.693223474	E
17	159.9343317	1.421048764	E
18	162.5031964	3.867893565	E
19	227.8997024	7.81520155	SE